JOURNAL OF GEOPHYSICAL RESEARCH, VOL. 112, C03S14, doi:10.1029/2006JC003515, 2007

Simulation and characterization of the Adriatic Sea mesoscale variability

Benoit Cushman-Roisin,[1] Konstantin A. Korotenko,[1] Camelia E. Galos,[1] and David E. Dietrich[2]

Received 6 February 2006; revised 19 October 2006; accepted 28 December 2006; published 24 March 2007.

[1] This paper presents simulations of the Adriatic Sea using the DieCAST model applied on a 1.2–min grid (about 2–km resolution). The simulations resolve the mesoscale variability because the grid size falls below the first baroclinic deformation radius (about 5–10 km) and DieCAST has very low horizontal dissipation. The model is initialized with seasonally averaged temperature and salinity data and forced with climatological winds and surface buoyancy fluxes (both heat flux and evaporation minus precipitation). River discharges are varied daily according to a perpetual year for every river, and the open-boundary conditions at Otranto Strait are obtained by nesting in two larger-scale models. The present simulations demonstrate that the DieCAST model allows mesoscale instabilities to develop at length scales of 5–20 km and over time scales of a few days. The simulated variability exhibits pronounced similarities with the actual mesoscale variability, in terms of location, nature and temporal evolution of the features. Meanders, swirls and eddies are noted along the relatively smooth Italian coast while offshore jets and filaments better describe the mesoscale activity along the more rugged coast of Croatia. In sum, DieCAST is highly suitable for the study of mesoscale variability in the Adriatic Sea. The present simulations also show that the seasonal hydrography of the Adriatic Sea is intrinsically unstable to mesoscale perturbations, and that the mesoscale variability along the Italian coast is the result of baroclinic instability of the Western Adriatic Current. It is shown how the properties of this instability are related to the local bottom topography.

Citation: Cushman-Roisin, B., K. A. Korotenko, C. E. Galos, and D. E. Dietrich (2007), Simulation and characterization of the Adriatic Sea mesoscale variability, *J. Geophys. Res.*, *112*, C03S14, doi:10.1029/2006JC003515.

1. Introduction

[2] The Adriatic Sea basin has been described in countless previous papers, and it suffices here to state that it is an elongated semienclosed sea with varied topography (Figure 1). Its circulation is driven by four distinct types of forcings [*Poulain and Raicich*, 2001]: wind stress, freshwater runoff, surface buoyancy fluxes, and exchange through the Strait of Otranto. The energetic bora, sirocco, maestrale and libeccio winds are episodic events that perturb the otherwise seasonally varying circulation; significant freshwater runoff along the rim of the basin, especially by the Po River in the northeastern corner [*Raicich*, 1994, 1996; *Sekulić and Vertačnik*, 1996] create important baroclinic pressure forces in the coastal areas; and, surface buoyancy fluxes include heating, cooling, evaporation and precipitation that drive additional motions. These forcing mechanisms vary not only seasonally but also on shorter time scales: Meteorological events bring winds and buoyancy fluxes that last but a few days [*Jurčec and Brzović*, 1995; *Supić and Orlić*, 1999], while the Po River discharge can fluctuate significantly within a single week [*Artegiani et al.*, 1993]. In addition, these strong events generate significant density perturbations and currents that require a few inertial periods for adjustment and may later succumb to their own barotropic–baroclinic instabilities. The result, as seen in satellite images [*Borzelli et al.*, 1999; *Cushman-Roisin et al.*, 2001] is intense variability on time scales ranging between a day and a week. The corresponding length scale is 10–40 km, i.e. several times the internal radius of deformation, which in the Adriatic can be as short as 5 km [*Paschini et al.*, 1993; *Cushman-Roisin et al.*, 2001].

[3] General descriptions of the dynamics of the Adriatic Sea have been provided over the years by *Buljan and Zore-Armanda* [1976], *Artegiani et al.* [1997a, 1997b] and *Cushman-Roisin et al.* [2001]. While these studies placed the focus on the general circulation and its seasonal variations, observations reveal that the Adriatic Sea is replete with mesoscale variability, about the dynamics of which much less is known.

[4] The best source of available data on the mesoscale in the Adriatic consists in satellite images of the sea surface

[1]Thayer School of Engineering, Dartmouth College, Hanover, New Hampshire, USA.
[2]Department of Mechanical Engineering, University of New Mexico, Albuquerque, New Mexico, USA.

0148-0227/07/2006JC003515$09.00

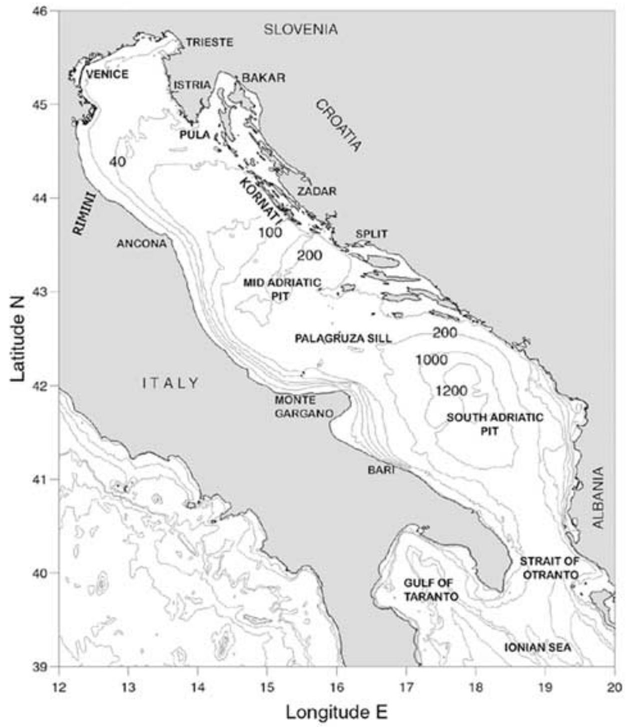

Figure 1. Geography and bathymetry of the Adriatic Sea. Depth contours are in meters.

temperature, color and chlorophyll. *Barale et al.* [1984] presented a series of images of diffuse attenuation coefficient (color) and apparent temperature collected by the CZCS during the winter of 1978–79. These revealed the meandering pattern of the Westerm Adriatic Current (WAC) in the middle and southern basins, a similar meandering of the northward coastal flow along the Albanian coast, and a complex circulation in the northern basin. Unfortunately, no good picture was presented for the Croatian coast, presumably because of cloud cover during the period of observation. Furthermore, these authors refrained from inferring any dynamics from the images. A subsequent article by *Barale et al.* [1986] presented additional images of the surface color field in the northern Adriatic and correlated the observed width of the Po River plume with in-situ river outflow discharges. Similarly, *Kuzmić* [1991, 1993] rationalized pigment concentration images derived from CZCS data over the northern Adriatic in terms of bora events, pointing to the crucial role played by the horizontal shear (curl) in the bora wind field.

[5] Satellite images revealing information in Croatian waters have been presented by *Borzelli et al.* [1999], who compiled and discussed sea surface temperature distributions from AVHRR measurements. This study focussed on the existence of several cold-water filaments originating from the Croatian coast and extending offshore across the Adriatic. The strongest member of this group appears to be the one in the middle Adriatic that follows the topographic escarpment forming the northern side of the Mid-Adriatic Pit, where the bottom drops abruptly from 100 to 200 m (Figure 1). They named it the Mid-Adriatic Filament (MAF). Rough cross-correlation of SST features in sequential images led the same authors to estimate that velocities in this jet can reach 10 to 20 cm/s, even under weak winds. They also speculated that the large temperature contrast between the MAF and ambient waters creates baroclinic pressure forces leading to geostrophic adjustment and that this adjustment must be significantly controlled by the underlying bottom slope.

[6] From these and similar sets of satellite images, the mesoscale structures of the Adriatic Sea appear to have the following properties, depending on the region. The Italian side has periodic meanders and eddies of identifiable wavelength, with a hint of development during calm periods; this is symptomatic of baroclinic instability in a relatively pure form. In contrast, the Croatian side has jets and filaments that tend to vary in speed and length of penetration but not in location; there are strong hints that topographic control plays a significant role in creating and guiding these jets. The southern Adriatic basin is characterized by instabilities of its two buoyant coastal currents (along Italy and Albania) and the instability of the South Adriatic Gyre. Finally, the northern basin, which is often affected by all three types of forcings simultaneously, exhibits complex behavior.

[7] However, all these satellite images merely provide horizontal patterns and time scales, not revealing much about the nature of the subsurface waters and the associated mesoscale currents. A discussion of the mesoscale activity from in-situ measurements has only been attempted twice. *Kastanos and Ferentinos* [1991] analyzed currentmeter data taken from the Strait of Otranto and noted current fluctuations in the shear zone separating the inflowing and outflowing waters. They ascribed these fluctuations to mesoscale eddies and near-inertial waves. Later, *Paschini et al.* [1993] reported on the first mesoscale experiment conducted on the Italian side of the middle Adriatic, during a four-day period in November 1988. The chief results were the observations of mesoscale eddies 10–25 km in diameter, with speeds ranging from 1 to 10 cm/s, and a vertical structure best corresponding to the second-baroclinic mode. Finally, not addressing directly mesoscale motions but nonetheless providing a measure of their variability are drifter tracks and maps of mean eddy kinetic energy derived from those tracks [*Poulain*, 1999, 2001]. These tracks show numerous loops, and eddy-kinetic-energy maps reveal several 'hot spots', including one off mid-Croatia in most seasons and one over the northern rim of the Mid-Adriatic Pit in autumn.

[8] Recently, in 2003–04, several cruises have gathered data on the mesoscale variability in the northern and middle basins of the Adriatic [*Lee et al.*, 2005]. And, while these are providing an important new source of data, it is premature to discuss their findings. The numerical model presented below is in fact prepared as a platform for several future investigations on the mesoscale dynamics as observed during these recent observational campaigns.

[9] In sum, not much is known about the dynamics of the mesoscale variability in the Adriatic Sea. There are, however, hints that it plays a crucial role in the Adriatic circulation and ecosystem: Instabilities can mix nutrients between the coast and open sea; offshore jets can flush Croatian channels and bring water from deeper layers to the surface and out to the open sea; eddies and mushroom currents can create temporary frontal zones (with obvious

impacts on both acoustics and biology); and, mesoscale currents in response to wind events (which are missed in seasonal studies that use monthly averaged winds) can have long-lasting effects by generating vertical mixing that persists long after each wind event.

[10] Only one modeling study of the mesoscale variability has been published to date for the Adriatic Sea. This paper, by *Masina and Pinardi* [1994], applied the Harvard quasi-geostrophic model to the region delineated in the aforementioned mesoscale experiment by *Paschini et al.* [1993]. Remaining modeling studies of the Adriatic on time scales of a few days have dealt exclusively with wind events and/or anomalous Po River discharges [*Orlić et al.*, 1994; *Bergamasco and Gačić*, 1996; *Četina*, 1997; *Kourafalou*, 1999, 2001]. Also, these studies have been based on models too dissipative to allow the unrestrained development of mesoscale motions and of their subsequent instabilities, and their authors placed instead the focus on the steady-state response following the event under consideration. All other modeling studies of the Adriatic to date have been concerned exclusively with the seasonal variability, of either circulation [e.g., *Zavatarelli and Pinardi*, 1995; *Zavatarelli et al.*, 2002; *Zavatarelli and Pinardi*, 2003] or deep-water formation [e.g., *Vested et al.*, 1998; *Lascaratos and Mantziafou*, 2001].

[11] Our approach is to use a numerical model with the least possible amount of horizontal dissipation, in order to allow the instabilities of the flow to develop as freely as possible. The model must also be capable of handling abrupt topography, such as the steep channels and escarpments off the Croatian coast. Under these constraints, DieCAST [*Dietrich*, 1997] stands as the model of choice, because of its 4th-order resolution in the horizontal (allowing large Reynolds numbers at the grid level) and its *z*-level discretization in the vertical (best suited for the representation of topographic steps). The application of this model to the Adriatic basin must also insure that the grid resolution is sufficiently high to resolve scales below the radius of deformation, that is, a few kilometers.

2. Model Description

2.1. General Model Description

[12] The DieCAST ocean model (http://fluid.stanford.edu/yhtseng/research/DieCAST/users_manual.pdf) is a *z*-level, finite-difference, three-dimensional, primitive-equations, hydrostatic, Boussinesq model with very low dissipation thanks to a fully 4th-order numerical scheme and a weakly filtered leap-frog time integration. For details of the governing equations, the reader is referred to *Dietrich* [1997] and to Appendix A of the paper by *Staneva et al.* [2001], which presents an application to the Black Sea.

[13] The model calculates control-volume averages of horizontal momentum, potential temperature and salinity. The vertical velocity is derived from the incompressibility equation after preliminary calculation of the horizontal velocity in a way that forces the divergence of the barotropic mode to match that implied by the specified vertical velocity at the surface. This surface vertical velocity is prescribed as a combination of net evaporation minus precipitation (E−P) and freshwater discharge from river sources located around the basin perimeter. Along the bottom, which consists in a series of horizontal steps, the vertical velocity is set to zero.

[14] With careful consideration of inflow characteristics, outflow characteristics and development of the intermediate water mass in winter, the DieCAST model produces realistic coastal dynamics even in regions of tortuous bathymetry [*Sheng et al.*, 1998]. The version of the model used here relies on the rigid-lid approximation, which simplifies the implementation of open-boundary conditions. For the slow modes that dominate the general circulation, the surface elevation field is derived hydrostatically from the model-determined sea-surface pressure against the rigid lid.

[15] Such a barotropic mode specification implies weak vortex stretching, in agreement with the long-term condition in the actual sea. In the inviscid limit, even weak vortex stretching has significant effects in the long run because of spin-up of the net lateral inflow or outflow needed to maintain the surface level. The barotropic mode condition requires that the pressure at the model rigid-lid satisfies a Poisson equation derived from the incompressibility and horizontal momentum equations. The hydrostatic equation then determines pressure everywhere else and may also be used to determine the hydrostatically equivalent free-surface height [cf. *Dietrich*, 1997]. The Poisson equation is solved by an efficient EVP elliptic solver [*Dietrich*, 1981; *Roache*, 1995]. Density is obtained from a nonlinear equation of state relating density to potential temperature, salinity and pressure (courtesy D. Wright, Bedford Institute, Dartmouth, Nova Scotia).

[16] Fourth-order accurate control volume approximations are used for all advection and horizontal pressure-gradient terms, except adjacent to boundaries where second−order accuracy is used. All control volumes are collocated (viz., momentum, energy, salinity equations are all applied on the same control volume). The incompressibility condition is applied to velocity components at control volume faces, thus requiring interpolation of nearby control-volume averaged velocities to the cell faces.

[17] After adjusting for incompressibility on the "C" grid (cell faces), the resulting adjustments are interpolated back to the collocated Arakawa "A" grid [*Dietrich*, 1997]. These and all other interpolations and finite-difference approximations (except the small dissipative terms and the hydrostatic vertical pressure gradient), are calculated with fourth-order accuracy. The Coriolis terms are evaluated on the *A* grid, thus having no spatial interpolation error, which is a significant advantage for such a dominant term.

[18] Surface boundary conditions are applied for heat and freshwater exchange with the atmosphere, as done in D. E. Dietrich et al. (Nonlinear Gulf Stream interaction with deep currents: Observations and a numerical simulation, submitted to *Ocean Modelling*, 2004). An advantage of this prescription is its avoidance of damping of surface fronts or transient eddies. The derived surface fluxes result in precise duplication, in a multiyear ensemble-average sense, of the observed annual cycle surface climatology (no damping or phase lag).

2.2. Model Adaptation to the Adriatic Sea

[19] The DieCAST model has already been applied once to the Adriatic Sea [*Dietrich et al.*, 2002], but this earlier implementation devoted to a study of the seasonal variability

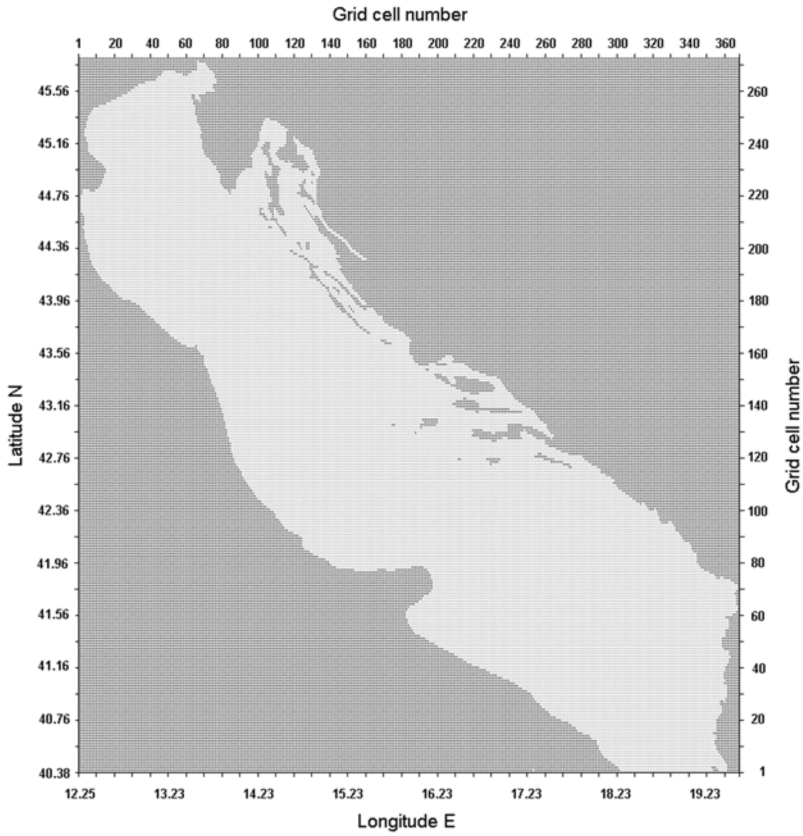

Figure 2. The 1.2-min model grid, showing the model's horizontal resolution, with numerous islands and channels.

of the circulation was performed on a grid (2.5 min horizontal resolution) too coarse to simulate adequately the mesoscale variability. Thus, we chose here to double that horizontal resolution by taking a mesh of 1.2 minute (1/50°). The overall dimension of the mesh is 370 × 272, covering the the entire Adriatic basin from 12.25° to 19.6°E and from 40.4° to 45.8°N. This resolution allows for a faithful representation of the larger and intermediate-size islands and channels in the Adriatic, especially along the Croatian coast (Figure 2), none of which were retained by *Dietrich et al.* [2002].

[20] The model has 20 unevenly spaced levels in the vertical, with interfacial depths at 0, 4.2, 9.4, 15.9, 23.8, 33.6, 45.7, 60.7, 102, 130, 165, 208, 261, 326, 404, 506, 629, 781, 969 and 1200 m. Smaller intervals near the surface were chosen for better representation of surface processes. Dense bathymetry data were provided by Dr. Vlado Malačič of the National Biology Institute in Piran, Slovenia and was initially converted to a finite-element mesh [*Cushman-Roisin and Naimie*, 2002] before being interpolated onto the present finite-difference grid and fitted to the selected *z*-levels. The resulting model topography is displayed in Figure 3.

[21] The seafloor is thermally insulated and allows no slip. A standard quadratic-drag coefficient equal to 0.002 is used throughout. In the staircase representation of the topography, the bottom drag applies to the momentum exchange (shear stress) along the horizontal side of each step, while there is no lateral stress against the vertical portion of each step (because this would generate undesirable horizontal dissipation).

[22] Horizontal viscosity and diffusivity are set to a constant value of 10 m^2/sec, while vertical viscosity and diffusivity obey formulas given in Appendix B of *Staneva and Stanev* [1997]. In brief, these formulas are the sum of a minimum laminar viscosity, a standard *Pacanowski and Philander* [1981] mixing parameterization dependent on the local Richardson number, and a small third term depending on the vertical spacing and grid Reynolds number designed to avoid overshoots by vertical advection [*Roache*, 1976], while producing extremely weak vertical mixing necessary to maintain the properties of intermediate water

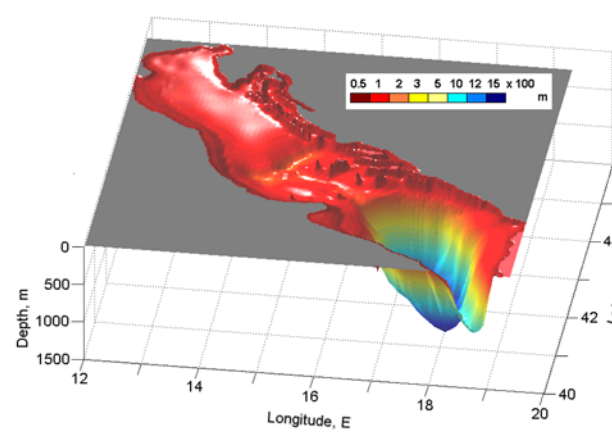

Figure 3. The model topography.

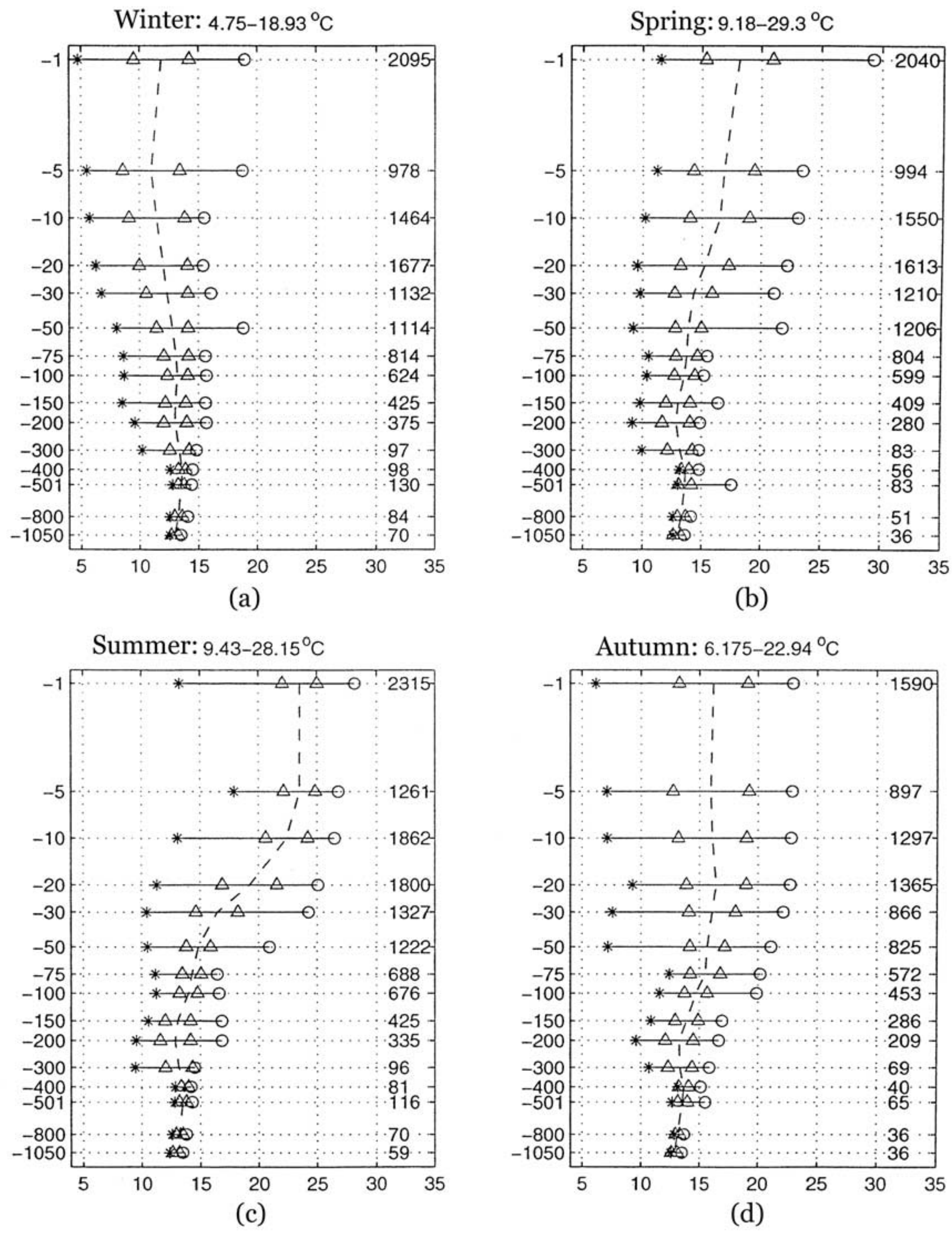

Figure 4. Seasonal vertical profiles of temperature in the Adriatic Sea according to $DADB_{raw}$: (a) winter, (b) spring, (c) summer, and (d) autumn. The symbols represent the following: vertical dashes, mean value; asterisks, minimum; open circles, maximum; open triangles, standard deviation [from *Galos*, 2000].

masses (with vertical eddy viscosity and diffusivity at near-laminar values of O(0.01 cm^2/s) for most of the water below a thin mixed layer). Such small values are implied by observed formation and maintenance throughout the year of the thin Cold Intermediate Layer in the Black Sea [*Staneva et al.*, 2001], which, being near the same latitude, is similar to the Adriatic Sea with respect to vertical mixing. Further, the higher resolution used in the present model reduces the appropriate subgridscale vertical mixing.

3. Hydrographic Database

[23] To initialize DieCAST for simulations of the Adriatic Sea, two basic collections of temperature and salinity measurements, the Mediterranean Oceanic Data Base

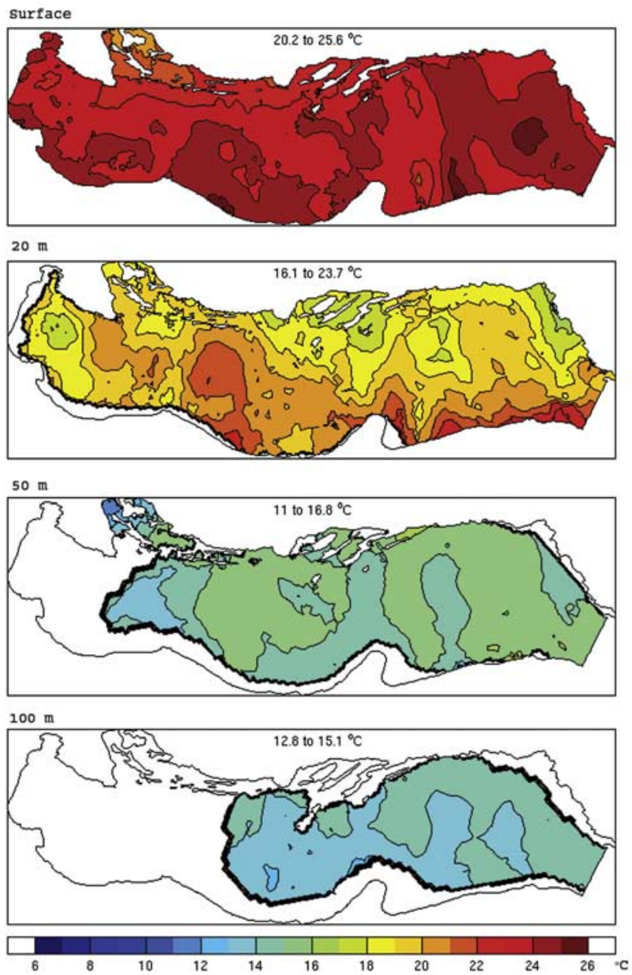

Figure 5. Temperature distributions at selected depths during summer, according to DADB [from *Galos*, 2000].

(MODB) and the Adriatic Sea Temperature, Oxygen and Salinity Data Set (ATOS2), were merged. MODB [*Brasseur*, 1995; *Brasseur et al.*, 1996] comprises temperature (T) and salinity (S) observations across the entire Mediterranean basin with the exception of coastal zones, containing a total of 22646 measurement points inside the Adriatic Sea with at least one valid entry, T or S. ATOS2 [*Artegiani et al.*, 1997a] is a compilation of 34964 temperature and salinity measurements at all depths, both in the open sea and near the coasts.

[24] The merging of MODB and ATOS2 gave rise to two problems: redundancy and uneven space-time distribution of the data. To overcome the former, duplicates were eliminated, and only those observations that were independent in space and time were retained. The resulting data set left some regions of the Adriatic with few data during certain months of the year and, as the goal was to create a climatological database, the monthly files were grouped according to the seasons, as defined in previous studies of the Adriatic Sea [*Zore-Armanda*, 1969; *Gačić et al.*, 1997]: winter – from January to March, spring – from April to June, summer – from July to September, and autumn – from October to December. This seasonally aggregated set of data – $DADB_{raw}$ – shows a more uniform distribution over the domain than the monthly data, both in space and in terms of the number of valid measurements for at least one parameter (T or S): 14349 locations in winter, 13523 in spring, 16168 in summer, and 11726 in autumn.

[25] In order to make the hydrographic observations comprehensive and useful, it is necessary to map the temperature and salinity data from the scattered measurements locations onto a structured grid by means of averages or interpolations. Because most of the observations were taken at depths of 0, 5, 10, 20, 30 m etc., these depths naturally forced the selection of the most meaningful levels for aggregation of the data in the vertical, and binning of $DADB_{raw}$ was performed in the following depth intervals: 0–2.5 m, 2.5–7.5 m, 7.5–14 m, 15–25 m, 26–34 m, 35–65 m, 65–85 m, 85–115 m, 115–185 m, 185–250 m, 251–350 m, 351–450 m, 451–601 m, 602–999 m and 850–1250 m. This offers the added advantage of generating a data set on a vertical grid that avoids relying on preconceived notions about vertical stratification, except for allowing larger gradients near the surface. As an illustration, Figure 4 shows the statistics of the vertical temperature profile for the four seasons.

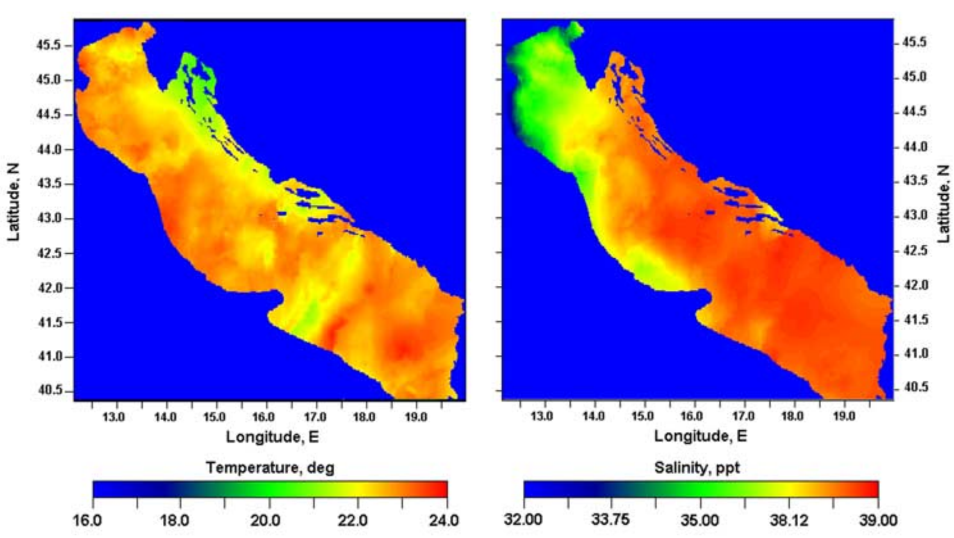

Figure 6. Surface temperature and salinity distribution for summer initialization.

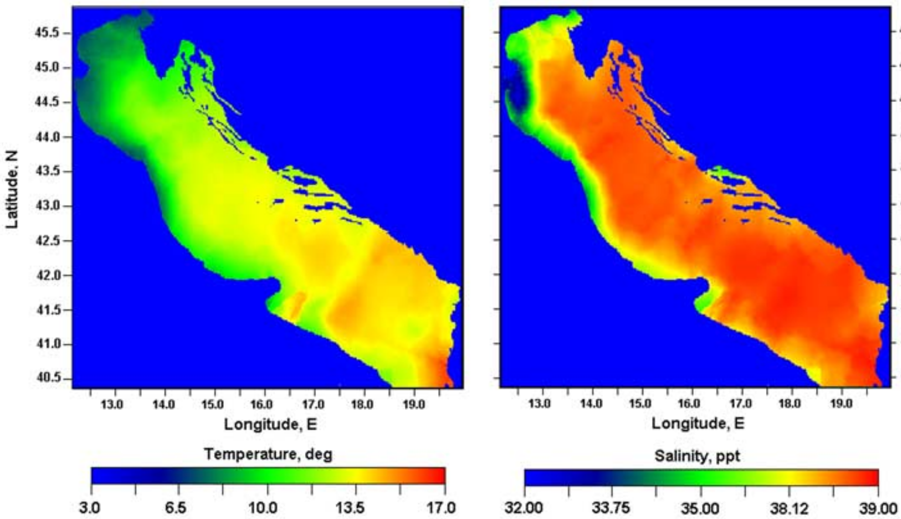

Figure 7. Surface temperature and salinity distribution for winter initialization.

[26] Once binned in the vertical, the T and S data were objectively interpolated in the horizontal on a finite-element mesh, with gradually finer resolution toward the coasts (same grid as in *Cushman-Roisin and Naimie* [2002]). This interpolation was carried in four-dimensional space (3D + time) using the OAX5 method developed at the Bedford Institute of Oceanography (http://www.mar.dfo-mpo.gc.ca/science/ocean/coastal_hydrodynamics/Oax/oax.html) based on the approach of *Bretherton et al.* [1976]. The parameter selection for the OAX interpolation is discussed by *Galos* [2000], and the OAX-estimated values of T and S all lie within 10% from the local mean values. In a final step, vertical density inversions were removed by means of vertical average of the data at those locations.

[27] Figure 5 displays temperature distributions at selected depths during summer, while Figures 6 and 7 show the temperature and salinity distributions at the sea surface during summer (Figure 6) and winter (Figure 7). Descriptions of these fields have been presented by *Artegiani et al.* [1997a] and *Galos* [2000]. The figures are merely shown here to illustrate the type and level of detail used for the initialization of the present model. It is noteworthy to note that, because those initialization fields are constructed from climatological data, they are necessarily very smooth. This is done on purpose so that the ensuing mesoscale variability simulated by the model can be characterized as intrinsic variability. By contrast, initialization by actual satellite SST distributions would have resulted in externally forced variability.

[28] For additional details on data processing and data statistics, the reader is referred to *Galos* [2000]. The Dartmouth Adriatic Data Base (DADB) can be downloaded from the internet (http://thayer.dartmouth.edu/other/adriatic/databanks/hydrography/hydrography.html). DADB interpolated on the model grid presented in Figure 2 is used to initialize the DieCAST model.

4. Forcings and Open-Boundary Condition

[29] As mentioned in the introduction, there are three types of forcings acting on the Adriatic Sea: river runoff, surface winds, and surface buoyancy fluxes, all of which are included in the present model. Freshwater fluxes from the 38 largest rivers around the perimeter of the basin are

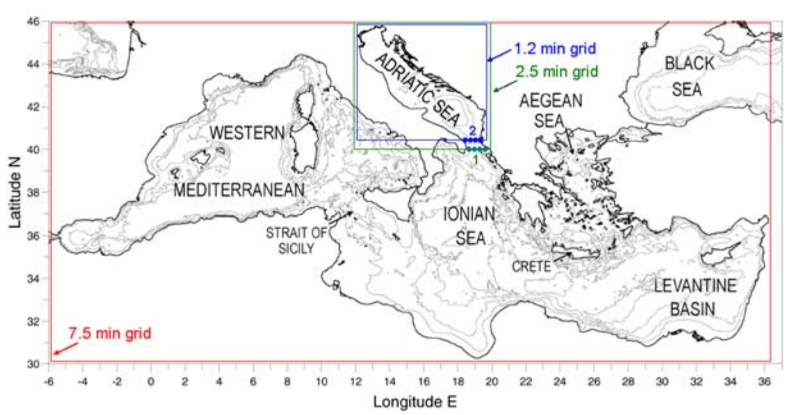

Figure 8. Hierarchy of nested grid, from a 7.5-min grid covering the entire Mediterranean Sea to 1.2-min grid of the present Adriatic model.

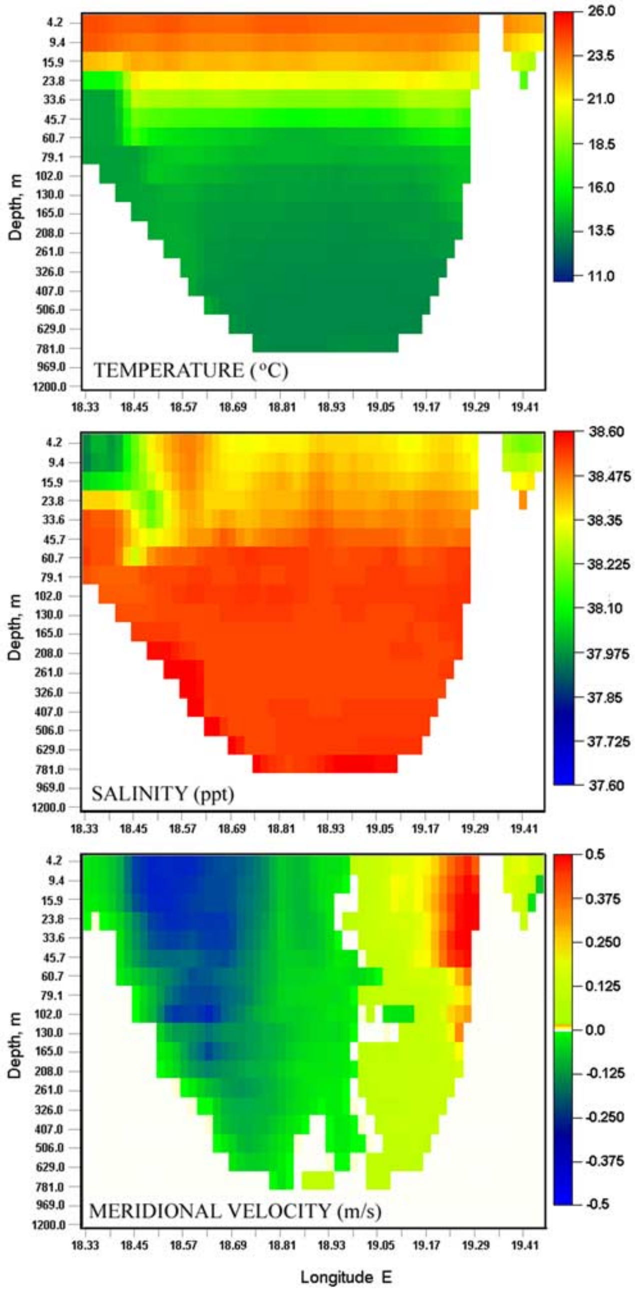

Figure 9. Open-boundary conditions at the Strait of Otranto at Day 183.

specified from climatological data sets [*Raicich*, 1994, 1996], which were interpolated to create perpetual annual cycles of daily values. River runoff is implemented in the model as a freshwater source in the topmost level of the grid cell closest to the river mouth. An exception is made for the Po River because of its size: Its discharge is divided among its four branches, and the discharge at each mouth is spread over the three closest grid cells.

[30] For surface winds, the model is spun up with the climatological wind data of *Hellerman and Rosenstein* [1983]. Once spun up, the model may be forced by actual wind stress to simulate any desired wind event. Monthly climatological surface heating, net precipitation minus evaporation (E−P) is taken from *Artegiani et al.* [1997a, Table 3].

[31] Significant exchange with the Mediterranean Sea occurs through Otranto Strait. In addition to a possible self-cancelling pair of inflow and outflow, there is a net volume outflow from the Adriatic Sea equal to the net input from rivers plus precipitation minus evaporation. Therefore, the model boundary across Otranto Strait (placed at 40.4°N in the model) must remain open. In order to simulate most realistically the inflows and outflows through the strait, the model is nested in a hierarchy of two larger models, as shown in Figure 8. The next larger model has a coarser resolution of 1/24° (2.5 minutes; model of *Dietrich et al.* [2002]) and covers an area a little larger than the high-resolution grid. It is run with climatological forcing only and receives its open-boundary conditions from a Mediterranean model with 1/8° (7.5-minute) resolution.

[32] The open-boundary conditions of each embedded model consist in an interpolation of the normal velocity, zero tangential velocity and the following condition on temperature and salinity: upstream value for outgoing flow and persistence for ingoing flow. An example of the distributions of normal velocity, temperature and salinity across Otranto Strait (line 2 on Figure 8) are shown in Figure 9.

5. Simulated Mesoscale Variability

[33] The model is spun up from rest and with temperature and salinity from the climatological summer data of *Galos* [2000]. By the fifth day of the simulation, the disjointed aspects of the initial fields have diffused, and subsequent days reveal new developments, including some mesoscale instabilities. The spin-up was continued for a total of 43 days, by which time the kinetic energy in the currents had become nearly stationary. The 43rd day of simulation is arbitrarily identified with Julian Day 183 (2 July), the middle of the calendar year and typical of the summer season.

[34] At a qualitative level, the simulations appear realistic. The length scale of the meanders and vortices (a few tens of kilometers) and their time scale of evolution (a few days) correspond well to what is seen in satellite images [*Barale et al.*, 1986; *Borzelli et al.*, 1999]. The observed contrast between the Croatian and Italian sides is also found in the simulated patterns of mesoscale motions, with a preponderance of jets and cold filaments on the Croatian side and of meanders and eddies on the Italian side. Both types of structures, be they on the Croatian or Italian sides, are accompanied by relatively well defined fronts. These motions can be classified as mesoscale variability because their length scale corresponds to several times the internal radius of deformation, as baroclinic-instability theory predicts [*Cushman-Roisin*, 1994, p. 231].

[35] Thus, before identifying and investigating specific mesoscale features of the model results, two general conclusions can already be stated. First, the seasonal circulation of the Adriatic is unstable, and the manifestation of this instability is mesoscale variability. Second, the low-dissipation nature of the DieCAST model allows the development of these mesoscale motions.

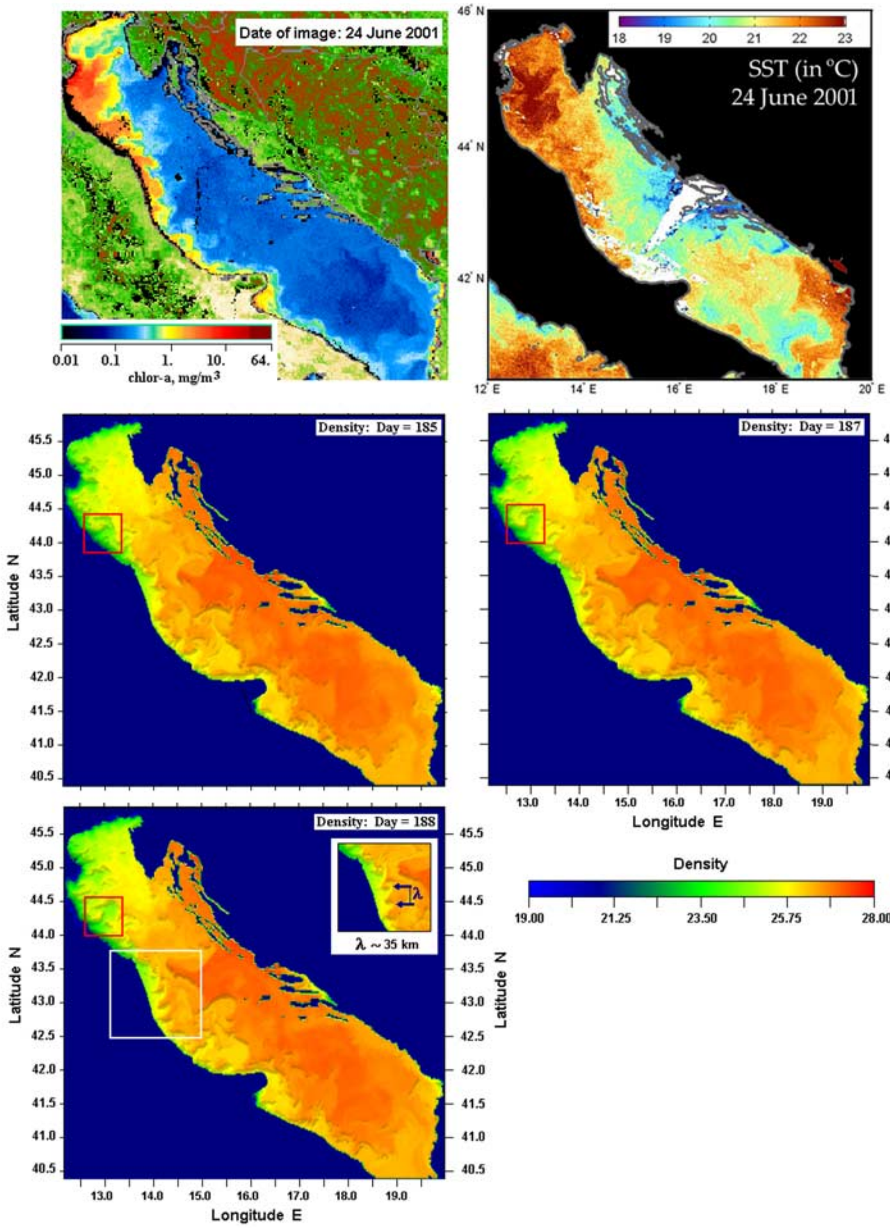

Figure 10. Development of the Rimini Squirt (red box) and triple meander south of Ancona (white box). The top panels are a SeaWiFS satellite image of the surface cholorophyl- a (left) and sea surface temperature (right), whereas the remaining three panels show the simulated surface density on days numbered according to the Julian calendar.

[36] We now turn to the identification and discussion of several specific features. First, we note the filamentous nature of the offshore, southwestward jet originating along the Croatian coastline at about 43°50′N (southern tip of Kornati). The forked-tongue appearance is strikingly similar to the one seen in the satellite image shown in *Borzelli et al.* [1999, Figure 3B].

[37] Next, at 44°N along the Italian coast, at the level of Rimini, lies a low-density protuberance that extends a quarter to a third of the distance across the basin. This is frequently seen in satellite images of surface chlorophyll in summer and autumn (top-left panel of Figure 10, as an example) and is also found in our numerical simulations (remaining panels of Figure 10). We shall call this feature the Rimini squirt. According to the simulations, the feature is episodic, consisting in a growing offshore jet terminating in a mushroom current, which eventually dissipates and leaves the stage free for another occurrence.

[38] Figure 11 shows the currents and relative-vorticity patterns associated with the squirt, which lies at both the surface and 23 m depth at the boundary between a cyclonic formation (red−yellow patch) to its left and an anticyclonic formation (blue patch) to its right. Close inspection of Figure 11 (aided by the positions of the added white and black dots, which represent the same latitude and longitude in each plot) reveals that the median line of the squirt lies more to the northwest at the surface than at 23 m. The net effect of this arrangement is a phase shift between the

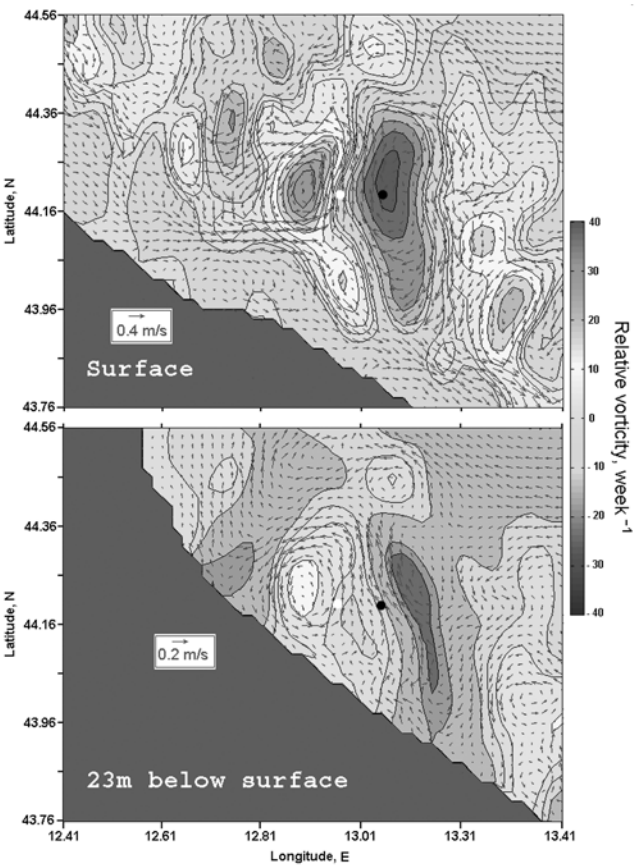

Figure 11. Currents (arrows) and relative vorticity (colors, in units of 1/week) at the surface (top) and at 23 m (bottom) on Julian day 187 of the simulation. The white and black dots in each panel lie on the same vertical, pointing to a lateral shift in relative velocity between the two levels. This shift fuels the instability.

surface and subsurface, such that the surface jet pulls offshore the lower-level cyclonic formation (yellow patch at 23 m) while the subsurface jet pulls offshore the upper-level anticyclonic formation (blue patch at the surface). And, since offshore displacement induces stretching in the lower level (because depth deepens offshore) and squeezing near the surface (because the buoyant coastal current becomes thinner offshore, under the sloping density surface associated with its geostrophic thermal wind), the result is amplification of the respective patterns: the subsurface cyclonic and surface anticyclonic formations both gain strength, and the jet increases over time. While this may appear complicated, it is none other than the vorticity dynamics at work in baroclinic instability (see *Cushman-Roisin* [1994, p. 226], where the "N" direction of Figure 16-1 in this book is offshore in the present application).

[39] Further, quantitative evidence that the baroclinic instability is the process at play here can be found in the comparison between relative vorticity (as plotted in color in Figure 11) and the amount of vertical stretching and squeezing involved during the squirt's formation. Baroclinic-instability theory [*Cushman-Roisin*, 1994] tells that both quantities should be comparable as it is the amount of vertical stretching ($\partial w/\partial z$) that is repsonsible for the generation of relative vorticity ($\partial v/\partial x - \partial u/\partial y$). With a rigid lid at the surface (w(surface) = 0), the amount of vertical stretching or squeezing taking place between the surface and 23 m depth is

$$\frac{\partial w}{\partial z} \simeq \frac{w(\text{surface}) - w(23\text{ m})}{23\text{ m}} = -\frac{w(23\text{ m})}{23\text{ m}}, \qquad (1)$$

which is negative for squeezing (upward velocity at depth) and positive for stretching (downward velocity at depth). Our model results indicate that the vertical velocity in the vicinity of the black dot in Figure 11 is positive, with a maximum of 6.6×10^{-4} m/s. This gives to the preceding ratio a value of -17.4 week^{-1}, which nicely falls within the range of relative vorticity values of -10 to -20 week^{-1} seen in the blue patch of Figure 11. The negative sign implies squeezing, as the thinning accompanying offshore displacement demands. By virtue of conservation of potential vorticity, squeezing generates anticylconic vorticity, which is exactly what is noted in Figure 11.

[40] Another frequent feature of the model simulations is a triple meander along the Italian coast immediately south of Ancona (the coastline kink at 43°40′N – see Figure 1). Like the Rimini Squirt, this, too, is noted in SeaWiFS satellite images. To see this, compare the top-left (SeaWiFS image) and bottom-right (model density) panels of Figure 10. To unravel the dynamics of this triple meander, we ran a simulation with an altered coastline in which the headland was removed and the coastline made more straight. The lack of significant change in the model simulations (not shown) indicates that the meandering is not tripped by the coastline curvature, and that another explanation is to be sought. According to the computer simulations, the wavelength λ of this meander set is about 35 km. In comparison, the internal radius of deformation R lies between 6 and 13 km (calculated from NH/f with H the water depth and $N = \sqrt{g\Delta\rho/\rho H}$, the Brunt-Vaisala frequency – Figure 12). Thus, the wavelength is several times the deformation radius, which agrees with the prediction of baroclinic-instability theory [*Cushman-Roisin*, 1994,

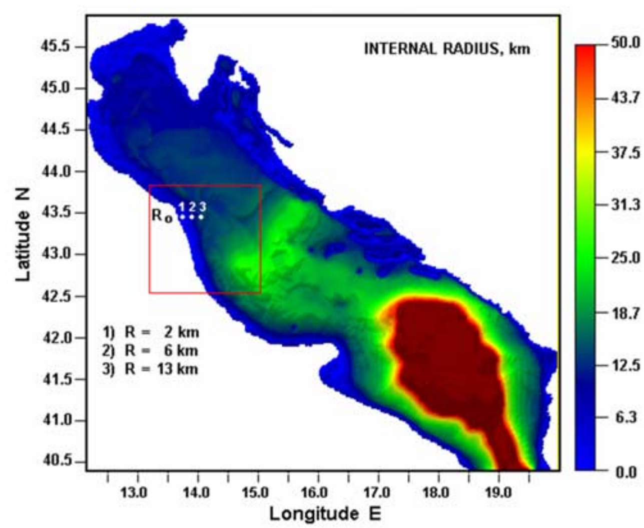

Figure 12. Values of the internal radius of deformation determined from the vertical density structure in the simulated fields.

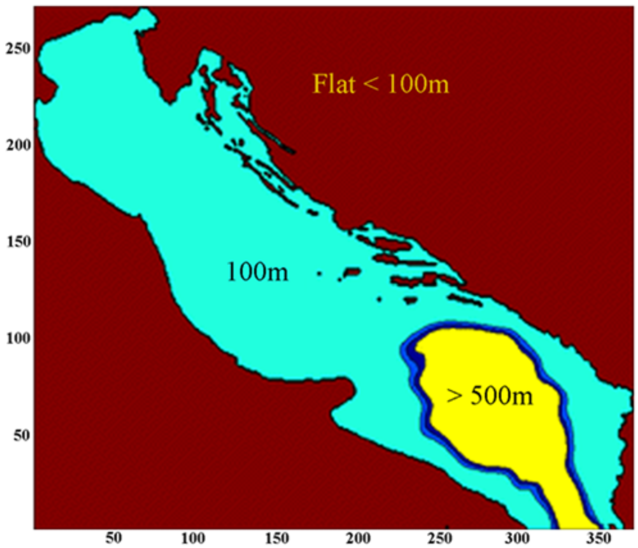

Figure 13. Altered bottom topography. All depths less than 100 m were increased to 100 m, in order to make the bottom flat near the coasts.

p. 231]. Although this relation does not offer a firm proof, baroclinic instability is the most likely cause of the meandering pattern.

[41] In an effort to learn more about the dynamics of these instabilities, we ran an experiment with altered bottom topography: All depths less than 100 m were deepened to 100 m (Figure 13), so that the coast turned into a 100 m-high vertical wall and the bottom became flat in broad regions along the coasts. The results (Figure 14) show that the three meanders still exist, continue to have the same wavelength but now reach larger amplitudes. Physically, offshore displacement is less restrained over a flat bottom than on a sloping shelf because it is not accompanied by vertical stretching and consequent relative-vorticity development, as required by potential-vorticity conservation. The offshore-sloping bottom in the actual basin thus acts as a restraining mechanism that limits the amplitude of the meandering, and such a charateristic corroborates the identification of the variability as baroclinic instability because it follows the theoretical result of *Gill et al.* [1974]. That the wavelength is unchanged further points to baroclinic instability, which says that the most unstable wavelength depends on the vertical stratification (via the internal radius of deformation R) and not on the bottom slope.

[42] Finally, another mesoscale feature generated by the model that appears to correspond well to an observed feature is the front anchored near the southern tip of the Croatian island chain of Kornati at 43.5°N and extending southwestward across half the basin (as evidenced by the sharp red-to-orange contrast in the density distribution in the lower panels of Figure 10). The position of this front, where the northwestward flow along the Croatian coast makes an abrupt left-hand turn, corresponds to the northern flank of the Mid-Adriatic Pit (Jabuka Pit), which is a steep escarpment with depth rising from more than 250 m to less than 100 m. The geostrophic jet accompanying this front is most likely none other than the Mid-Adriatic jet noted in satellite images of the sea surface temperature by *Borzelli et al.* [1999]. The location of the front and jet points to topographic steering: As argued by *Carnevale et al.* [1999], conservation of potential vorticity in the presence of vertical squeezing on the shallower side to north and stretching on the deeper side to the south generates a pattern with anticyclonic vorticity on the shallower side and cyclonic vorticity on the deeper side, which together form a jet flowing with the shallower water on its right, as observed in our simulations. The sharpness of the front reflects the steepness of the escarpment.

6. Conclusions

[43] The DieCAST model has been used to simulate the mesoscale variability of the Adriatic Sea, and the computa-

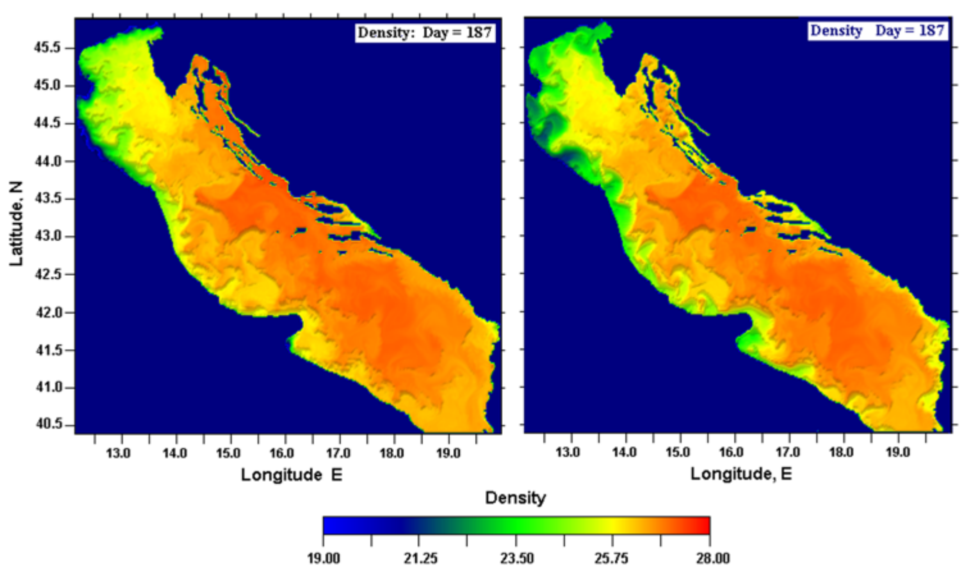

Figure 14. Comparison of the three-meander pattern with actual bathymetry (left) and flattened bottom (right) on Day 187 of the simulations. With flat bottom, the meanders retain their wavelength but reach larger amplitudes.

tions are deemed successful in the sense that the simulated variability reproduces well a number of features observed in satellite images. This performance can be attributed to the following combination of characteristics: The low-dissipation nature of the model (which is 4th-order accurate in the horizontal), the high numerical resolution of the mesh (1.2 min, about 2 km), and the initialization of the model with seasonal hydrography. The present simulations add to the body of literature showing the suitability of DieCAST in simulating mesoscale variability in various oceanic regions, namely in the Gulf of Mexico [*Dietrich et al.*, 1997], the California Current system [*Haney et al.*, 2001], the Black Sea [*Staneva et al.*, 2001; *Korotenko et al.*, 2003], and the Mediterranean Sea [*Fernandez et al.*, 2007].

[44] A task preliminary to the model implementation consisted in establishing an aggregate seasonal database for temperature and salinity in the Adriatic Sea. This comprehensive database, called the Dartmouth Adriatic Data Base, is a significant product by itself and is made available to the oceanographic community (http://thayer.dartmouth.edu/other/adriatic/databanks/hydrography/hydrography.html).

[45] After a spin-up period of about 20 days, the model began to produce realistic mesoscale variability, and further spin-up was conducted for a total of 43 days to ensure stabilization in the level of kinetic energy. Then, the study proceeded with the investigation of several specific mesoscale features produced by the model that have clear correspondence with actual features observed in the Adriatic Sea.

[46] First, the Rimini Squirt, an episodic jet shooting offshore from the Italian coast at 44°N and terminating in a mushroom current, was diagnosed as a manifestation of baroclinic instability of the coastal cuurent. Farther south along the Italian coast, a set of three meanders was investigated, and it was concluded that this formation is not tripped by the Ancona promontory immediately upstream, that its wavelength is several times the internal radius of deformation, pointing out to baroclinic instability as its most likely cause, and that its offshore amplitude is strongly affected by the bottom slope in the area. Finally, the front across the basin at 43.5°N was found to be anchored on the topographic escarpment of northern flank of the Mid-Adriatic Pit (Jabuka Pit), and its existence is owed to potential-vorticity conservation in the presence of vertical squeezing and stretching associated with the steep bottom.

[47] The present work lays the groundwork for a series of further applications of DieCAST to the Adriatic Sea. Worthy of future investigation are the wind-driven response of the sea to various types of wind events for which the Adriatic is notorious (bora, sirocco among others) and the response of the northern and middle basins to low and high discharges of the Po River. Particular events deserving close scrutiny because they were quite pronounced and were also well captured by field observations at the time of their occurrence are the bora event of 12–19 February 2003 and the episode of extremely low Po River discharge immediately followed by an intense sirocco during 11–23 July 2003, during which time the Western Adriatic Current was reversed and unusual upwelling was observed along the Italian coast [*Poulain et al.*, 2004].

[48] **Acknowledgments.** Support for this study was provided by the U.S. Office of Naval Research under grants N00014-93-1-0391 and N00014-02-1-0065 to Dartmouth College. The authors also wish to thank Vlado Malačič for providing bathymetry data and helpful discussions, Christopher E. Naimie for assistance with the conversion of some data set from an earlier, finite-element grid, Malcolm Bowman for thoughtful advice on the use of the DieCAST model, Miro Gačić for assistance with SeaWiFS images, and Elena Mauri for assistance with sea surface temperature images.

References

Artegiani, A., M. Gačić, A. Michelato, V. Kovačević, A. Russo, E. Paschini, P. Scarazzato, and A. Smirčić (1993), The Adriatic Sea hydrography and circulation in spring and autumn (1985–1987), *Deep Sea Res., Part II*, *40*, 1143–1180.

Artegiani, A., D. Bregant, E. Paschini, N. Pinardi, F. Raicich, and A. Russo (1997a), The Adriatic Sea general circulation. Part I: Air-sea interactions and water mass structure, *J. Phys. Oceanogr.*, *27*, 1492–1514.

Artegiani, A., D. Bregant, E. Paschini, N. Pinardi, F. Raicich, and A. Russo (1997b), The Adriatic Sea general circulation. Part II: Baroclinic circulation structure, *J. Phys. Oceanogr.*, *27*, 1515–1532.

Barale, V., P. Malanotte-Rizzoli, and M. Hendershott (1984), Remotely sensing the surface dynamics of the Adriatic Sea, *Deep Sea Res.*, *31*, 1433–1459.

Barale, V., C. R. McClain, and P. Malanotte-Rizzoli (1986), Space and time variability of the surface color field in the northern Adriatic Sea, *J. Geophys. Res.*, *91*, 12,957–12,974.

Bergamasco, A., and M. Gačić (1996), Baroclinic response of the Adriatic Sea to an episode of bora-wind, *J. Phys. Oceanogr.*, *26*, 1354–1369.

Borzelli, G., G. Manzella, S. Marullo, and R. Santoleri (1999), Observations of coastal filaments in the Adriatic Sea, *J. Mar. Syst.*, *20*, 187–203.

Brasseur, P. (1995), Free data offered to researchers studying the Mediterranean, *Eos Trans. AGU*, *76*(37), 363.

Brasseur, P., J. M. Beckers, J. M. Brankart, and R. Schoenauen (1996), Seasonal temperature and salinity fields in the Mediterranean Sea: Climatological analyses of an historical data set, *Deep Sea Res.*, *43*, 159–192.

Bretherton, F. P., R. E. Davis, and C. B. Fandry (1976), A technique for objective analysis and design of oceanographic experiments applied to MODE-73, *Deep Sea Res.*, *23*, 559–582.

Buljan, M., and M. Zore-Armanda (1976), Oceanographical properties of the Adriatic Sea, *Oceanogr. Mar. Biol. Ann. Rev.*, *14*, 11–98.

Carnevale, G. F., S. G. Llewellyn, F. Smith, R. Crisciani, R. Purini, and R. Serravall (1999), Bifurcation of a coastal current at an escarpment, *J. Phys. Oceanogr.*, *29*, 969–985.

Četina, M. (1997), 3D mathematical modelling of the Po River inflow in the northern Adriatic, in *Water Pollution*, vol. 4, *Modelling, Measuring and Prediction*, edited by R. Rajar and C. A. Brebbia, pp. 637–646, Comput. Mech., Billerica, Mass.

Cushman-Roisin, B. (1994), *Introduction to Geophysical Fluid Dynamics*, 320 pp., Prentice-Hall, Upper Saddle River, N. J.

Cushman-Roisin, B., and C. E. Naimie (2002), A 3D finite-element model of the Adriatic tides, *J. Mar. Syst.*, *37*, 279–297.

Cushman-Roisin, B., M. Gačić, P.-M. Poulain, and A. Artegiani (2001), *Physical Oceanography of the Adriatic Sea: Past, Present and Future*, 304 pp., Springer, New York.

Dietrich, D. E. (1981), A program of elliptic solver development and implementation in semi-implicit numerical ocean circulation models, *JAYCOR Final Rep. J510-81-053/2192*, JAYCOR, La Jolla, Calif.

Dietrich, D. E. (1997), Application of a modified "A" grid ocean model having reduced numerical dispersion to the Gulf of Mexico circulation, *Dyn. Atmos. Oceans*, *27*, 201–217.

Dietrich, D. E., C. A. Lin, A. Mestas-Nunez, and D.-S. Ko (1997), Numerical study of Gulf of Mexico fronts and eddies, *Meteorol. Atmos. Phys.*, *64*, 187–201.

Dietrich, D., G. F. Carnevale, and P. Orlandi (2002), Adriatic simulations by DieCAST, in *Proceedings of Summer Program*, pp. 269–281, Cent. for Turbulence Res., Stanford Univ., Stanford, Calif.

Fernandez, V., D. E. Dietrich, R. L. Haney, and J. Tintore (2007), Mesoscale, seasonal and interannual variability in the Mediterranean Sea using the DieCAST ocean model, *J. Mar. Syst.*, in press.

Gačić, M., S. Marullo, R. Santoleri, and A. Bergamasco (1997), Analysis of seasonal and interannual variability of the sea surface temperature field in the Adriatic Sea from AVHRR data (1984–1992), *J. Geophys. Res.*, *102*, 22,937–22,946.

Galos, C. E. (2000), Seasonal circulation in the Adriatic Sea, M.S. thesis, 127 pp., Dartmouth Coll., Hanover, N. H.

Gill, A. E., J. S. A. Green, and A. J. Simmons (1974), Energy partition in the large-scale ocean circulation and the production of mid-ocean eddies, *Deep Sea Res.*, *21*, 499–528.

Haney, R. L., R. A. Hale, and D. E. Dietrich (2001), Offshore propagation of eddy kinetic energy in the California Current, *J. Geophys. Res.*, *106*(C6), 11,709–11,717.

Hellerman, S., and M. Rosenstein (1983), Normal monthly wind stress over the world ocean with error estimates, *J. Phys. Oceanogr.*, *13*, 1093–1104.

Jurčec, V., and N. Brzović (1995), The Adriatic bora: special case studies, *Geofizika*, *12*, 15–32.

Kastanos, N., and G. Ferentinos (1991), Mesoscale current variability in the Otranto Straits, Adriatic Sea, *J. Geophys. Res.*, *96*, 8741–8754.

Korotenko, K. A., M. J. Bowman, and D. E. Dietrich (2003), Modeling circulation and oil spill transport and dispersal in the Black Sea, *Oceanology*, *43*(4), 411–421.

Kourafalou, V. H. (1999), Process studies on the Po River plume, North Adriatic Sea, *J. Geophys. Res.*, *104*, 29,963–29,985.

Kourafalou, V. H. (2001), River plume development in semi-enclosed Mediterranean regions: North Adriatic Sea and northwestern Aegean Sea, *J. Mar. Syst.*, *30*, 181–205.

Kuzmić, M. (1991), Exploring the effects of bura over the northern Adriatic: CZCS imagery and a mathematical prediction, *Int. J. Remote Sens.*, *12*, 207–214.

Kuzmić, M. (1993), A satellite observation of the Adriatic Sea response to a spatially heterogeneous wind, *Geofizica*, *10*, 1–18.

Lascaratos, A., and A. Mantziafou (2001), Modeling of deep-water formation, Section 4.2 in *Physical Oceanography of the Adriatic Sea: Past, Present and Future*, edited by B. Cushman-Roisin et al., pp. 125–129, Springer, New York.

Lee, C. M., et al. (2005), Northern Adriatic response to a wintertime bora wind event, *Eos Trans. AGU*, *86*, 157–165.

Masina, S., and N. Pinardi (1994), Mesoscale data assimilation studies in the Middle Adriatic Sea, *Cont. Shelf Res.*, *12*, 1293–1310.

Orlić, M., M. Kuzmić, and Z. Pasarić (1994), Response of the Adriatic Sea to the bora and sirocco forcing, *Cont. Shelf Res.*, *14*, 91–116.

Pacanowski, R. C., and S. G. H. Philander (1981), Parameterization of vertical mixing in numerical models of tropical oceans, *J. Phys. Oceanogr.*, *11*, 1443–1451.

Paschini, E., A. Artegiani, and N. Pinardi (1993), The mesoscale eddy field of the Middle Adriatic Sea during fall 1988, *Deep Sea Res., Part I*, *40*, 1365–1377.

Poulain, P.-M. (1999), Drifter observations of surface circulation in the Adriatic Sea between December 1994 and March 1996, *J. Mar. Syst.*, *20*, 230–253.

Poulain, P.-M. (2001), Adriatic Sea surface circulation as derived from drifter data between 1990 and 1999, *J. Mar. Syst.*, *29*, 3–32.

Poulain, P.-M., and F. Raicich (2001), Forcings, in *Physical Oceanography of the Adriatic Sea: Past, Present and Future*, edited by B. Cushman-Roisin, M. Gačić, P.-M. Poulain, and A. Artegiani, pp. 45–65, Springer, New York.

Poulain, P.-M., E. Mauri, and L. Ursella (2004), Unusual upwelling event and current reversal off the Italian Adriatic coast in summer 2003, *Geophys. Res. Lett.*, *31*, L05303, doi:10.1029/2003GL019121.

Raicich, F. (1994), Note on the flow rates of the Adriatic rivers, *Tech. Rep. RF 02/94*, 8 pp., CNR Istituto Sperimentale Tallassografico, Trieste, Italy.

Raicich, F. (1996), On the fresh water balance of the Adriatic Sea, *J. Mar. Syst.*, *9*, 305–319.

Roache, P. J. (1976), *Computational Fluid Dynamics*, 446 pp., Hermosa, Albuquerque, N. M.

Roache, P. J. (1995), *Elliptic Marching Methods and Domain Decomposition*, 190 pp., CRC Press, Boca Raton, Fla.

Sekulić, B., and A. Vertačnik (1996), Balance of average annual fresh water inflow into the Adriatic Sea, *Water Res. Dev.*, *12*, 89–97.

Sheng, J., D. G. Wright, R. J. Greatbatch, and D. E. Dietrich (1998), CANDIE: A new of the DieCAST ocean circulation model, *J. Atmos. Oceanic Technol.*, *15*, 1414–1432.

Staneva, J. V., and E. V. Stanev (1997), Cold water mass formation in the Black Sea: Analysis on numerical model simulations, in *Sensitivity to Change: Black Sea, Baltic Sea and North Sea*, edited by E. Ozsoy and A. Mikaelyan, *NATO ASI Ser.*, *27*, 375–393.

Staneva, J. V., D. E. Dietrich, E. V. Stanev, and M. J. Bowman (2001), Rim current and coastal eddy mechanisms in an eddy-resolving Black Sea general circulation model, *J. Mar. Syst.*, *31*, 137–157.

Supić, N., and M. Orlić (1999), Seasonal and interannual variability of northern Adriatic surface fluxes, *J. Mar. Syst.*, *20*, 205–229.

Vested, H. J., P. Berg, and T. Uhrenholdt (1998), Dense water formation in the northern Adriatic, *J. Mar. Syst.*, *18*, 135–160.

Zavatarelli, M., and N. Pinardi (1995), The Adriatic Sea general circulation: Modelling with the Blumberg-Mellor model, *Ann. Geophys.*, *13*, suppl. II.

Zavatarelli, M., and N. Pinardi (2003), The Adriatic Sea Modeling System: A nested approach, *Ann. Geophys.*, *21*, 345–364.

Zavatarelli, M., N. Pinardi, V. H. Kourafalou, and A. Maggiore (2002), Diagnostic and prognostic model studies of the Adriatic Sea general circulation: Seasonal variability, *J. Geophys. Res.*, *107*(C1), 3004, doi:10.1029/2000JC000210.

Zore-Armanda, M. (1969), Temperaturni odnosi u Jadranskom Moru (Temperature relations in the Adriatic Sea), *Acta Adriatica*, *13*(5), 1–50.

B. Cushman-Roisin, C. E. Galos, and K. A. Korotenko, Thayer School of Engineering, Dartmouth College, Hanover, NH 03755-8000, USA. (benoit.r.roisin@dartmouth.edu)

D. E. Dietrich, Department of Mechanical Engineering, University of New Mexico, Albuquerque, NM 87131, USA.